Single-Stage Fuel Cell to Grid Interface With Multilevel Current-Source Inverters

Pablo Cossutta, *Member, IEEE*, Miguel Pablo Aguirre, *Member, IEEE*, Andrés Cao, Santiago Raffo, *Member, IEEE*, and María Inés Valla, *Fellow, IEEE*

***Abstract*—Renewable energy sources can be used for electric power generation to supply specific devices in distributed systems such as smart grids. Hydrogen fuel cells have proven to be an effective solution to produce electrical energy with fairly good efficiency and minimum environmental pollution. A single-stage solution to interconnect a fuel cell with a low-voltage distribution system is proposed in this paper. The traditional boost dc/dc converter plus voltage source inverter is replaced by a single-stage multilevel current-source inverter (MCSI). The MCSI can both interconnect to the grid and perform the maximum power point tracking algorithm. This novel single-stage converter approach provides active power to the grid, power factor compensation, and reduction of the line current harmonic content. The synchronization, modulation, and control scheme are implemented on a field-programmable gate array board using a fast-prototype high-level synthesis tool to reduce design time. Both simulation and experimental results show excellent behavior and fast dynamics while complying with IEEE and IEC harmonic content regulations.**

***Index Terms*—Field-programmable gate array (FPGA), fuel cells, grid interface, maximum power point tracking (MPPT), multilevel current-source inverter (MCSI).**

I. Introduction

RENEWABLE energy sources are one of the focal points of research in distributed power generation, attracting a significant amount of resources worldwide in the quest for new methods of energy generation and storage. Recent developments in hydrogen technologies have allowed the conversion between electric energy and hydrogen back and forth, increasing efficiency and reducing costs. In environmentally friendly applications, storing energy in the form of hydrogen and later transforming it to electrical energy is an excellent choice since hydrogen-based electric systems can be used as a substitute for large battery banks [1]–[3].

Manuscript received August 1, 2014; revised November 7, 2014, March 7, 2015, and April 12, 2015; accepted April 26, 2015. Date of publication May 18, 2015; date of current version June 26, 2015.

P. Cossutta, M. P. Aguirre, A. Cao, and S. Raffo are with the Centro de Investigación y Desarrollo en Electrónica Industrial (CIDEI), Instituto Tecnológico de Buenos Aires (ITBA), Buenos Aires, Argentina (e-mail: pcossutt@itba.edu.ar).

M. I. Valla is with the Instituto de Investigaciones en Electrónica, Control y Procesamiento de Señales (LEICI), Facultad de Ingeniería, Universidad Nacional de La Plata (UNLP), La Plata, Argentina, and also with the Consejo Nacional de Investigaciones Científicas y Técnicas (CONICET), Buenos Aires, Argentina (e-mail: m.i.valla@ieee.org).

Color versions of one or more of the figures in this paper are available online at http://ieeexplore.ieee.org.

Digital Object Identifier 10.1109/TIE.2015.2434800

The use of hydrogen as an energy storage method presents many advantages compared with batteries, particularly regarding lifetime, weight, and environmental safety. Rechargeable batteries such as sealed lead–acid, lithium-, or cadmium-based batteries contain toxic heavy metals and may cause serious environmental problems if they do not get regular maintenance or are not discarded with special care [4]. On the other hand, fuel cell technologies have proven to be an attractive power source because they are inherently clean, efficient, and reliable [5], [6]. These features make them a promising alternative to substitute the pollutant technologies in various applications such as automotive, portable power, remote generation, backup power, and distributed generation.

Furthermore, supercapacitors can be used to respond to rapid load changes or to start operation as soon as it is needed, compensating for the fact that fuel cells do not have the capability to respond immediately [7]. In addition, when a considerable proportion of the power is generated by renewable energy sources such as wind or solar sources, the electrical systems present continuous disturbances such as sags and swells, which directly affect the power quality [8], [9]. Aside from the ability of delivering energy from the fuel cell to the grid, power converters in conjunction with supercapacitors can help improve the power quality problems by acting as active filters, absorbing and releasing power much faster than traditional electrical regulators [10].

To achieve the highest possible efficiency, it is mandatory to use electronic converters in order to adapt the current and voltage provided by the cell to the requirements of the load or the grid. Distributed power generation should be injected by three-phase converters to avoid imbalances in an electric grid. Additionally, since the fuel cell stack delivers direct current (dc), which depends mostly on the temperature and fuel pressure, an electronic interface is required to match both the load and the operating conditions of the cell [11]. The electronic interface can modify the current sink from the cell stack depending on the voltage generated to obtain the maximum power at any time regardless of the operating condition [12], [13]. Power converters allow finding and tracking the maximum power point of operation not only of the cell stack but also of the whole system [6], [13], [14]. A better dynamic response can be achieved by controlling either the active or reactive power in both directions between the converter and the grid. Thus, power converters must have bidirectional power exchange capabilities in order to compensate reactive power. A particular subclass of power converters, called multilevel converters [15], offers major advantages in terms of versatility, dynamic response, reduction of

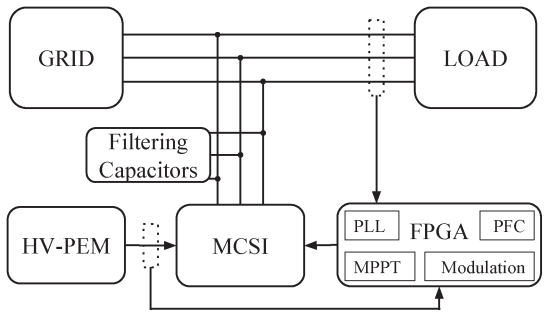

Fig. 1. System layout.

high-frequency electrical disturbances in the load generated by the commutation of the switches [16], reduction in the requirements of maximum voltage and/or current of the switches, and the possibility of fault-tolerant operation. The main drawback is the increased complexity of the power inverter [4], [17], [18].

Additionally, any grid-connected power inverter requires a synchronization method to track the main sequence, phase, and frequency of the grid voltage to be able to control the exchange of power between the electric system and the dc bus [19].

The speed and accuracy of the synchronization method directly impact on the performance of the inverter and the power quality of the grid; thus, it must be carefully designed and tested under the most severe fault conditions the system might undergo.

Control systems based on field-programmable gate arrays (FPGAs) allow high-speed data processing, variable bit accuracy, fault-tolerant architectures, and easily scalable designs. Regardless of these qualities, one of the most powerful advantages of an FPGA is the ability to compute all the converter control system blocks in parallel, saving time and increasing reliability [20]. In order to be scalable and comparable with the experimental results, simulation models in this paper consider the internal logic timing, the switches' behavior, and the saturation limits of the actual control and synchronization systems.

The interconnection of the fuel cell to the grid proposed in this paper consists of a single stage only built with a multilevel current-source inverter (MCSI). Since MCSIs can boost the input voltage, there is no need for a supplementary stage. Maximum power point tracking (MPPT) is also achieved by controlling the reference signals of the MCSI. This solution reduces the complexity and power losses while increasing the power density, efficiency, and reliability of the system.

II. System Description

A three-phase MCSI is used to inject the current provided by a proton exchange membrane (PEM)-type fuel cell to a 3×190 V_{LL}, 50-Hz, and three-phase utility grid, as shown in the basic schematic in Fig. 1.

An MCSI has three main advantages. First, it can be connected directly to the utility grid without any coupling inductors. Second, it can drain constant current from the fuel cell. Third, it requires smaller input voltage compared with traditional voltage inverters. Current source inverters (CSIs) have a large inductor on the dc side; this means that the current drained from the energy source has a low ripple. At the output, a small capacitor bank is required to smooth commutation currents, avoiding overvoltages due to inductances in the current path [15].

The control algorithms and modulation signals of the MCSI are implemented on an FPGA, as well as data acquisition and processing. A simple controller based on a Park transform (*dq0*) controlling the MCSI output current is enough to compensate both power factor and harmonics caused by the load on the current of the grid [21]. Moreover, the MPPT controller acts directly over the active power set point of the system. If required, a smart grid control can adjust the power provided to the grid to a suitable level.

A. MCSI

The schematic of the inverter is shown in Fig. 2. It consists of three identical modules with the capability of producing seven levels in the output current, as shown in Fig. 3. Each module has six switches with bidirectional voltage blocking capabilities and two inductors to balance the current through them. All the balance inductors are identical and carry the same average current, simplifying the design, construction, operation, and maintenance of the inverter. The current of each module can be balanced by the use of the well-known phase-shifted carrier sinusoidal pulsewidth modulation (PSC-SPWM) [15], [22], in which gate signals are calculated comparing the reference signals with three equally phase-shifted triangular waveforms. A block diagram of the PSC-SPWM is shown in Fig. 4, and the SPWM of the first module is displayed in Fig. 5.

Power converters can be classified into voltage-source inverters (VSIs) and CSIs depending on the topology of the power supply [23]. The implementation of the SPWM in a CSI is not as straightforward as that in a VSI. The gating signals for a VSI are generated by the comparison of one triangular carrier with three sine waves. The driving signals for a CSI need more logic manipulation to generate the desired current level at the load while assuring current continuity in all the inductors. First, the standard SPWM signals P_A, P_B, and P_C in Fig. 5(b) are generated by the comparison of one triangular with three sine waves. These phase signals are XORed two at a time to obtain a logic equivalent to the line-to-line voltage in a VSI. The obtained signals are ANDed with the required sign of the current in each phase, or its logic complement, to obtain the firing signals of upper or lower switches, respectively [as shown in Fig. 5(c)]. These signals cannot directly drive the gates of the insulated-gate bipolar transistors (IGBTs) since they generate zero states by turning off all switches [Time "z" in Fig. 5(c)], thus not allowing inductor's current continuity. The zero states generated by the SPWM logic should be recognized and replaced by adequate zero states, taking advantage of the redundancy of the CSI topology. A detailed analysis of the circuit topology and the modulation method can be found in [22].

Each module can produce zero-current state in three different ways by turning on both switches in any leg of the inverter. This adds two redundant states to the switching combinations, meaning that one of these available states can be chosen in order to reduce the overall amount of commutations during a cycle. The maximum instantaneous absolute value of the line

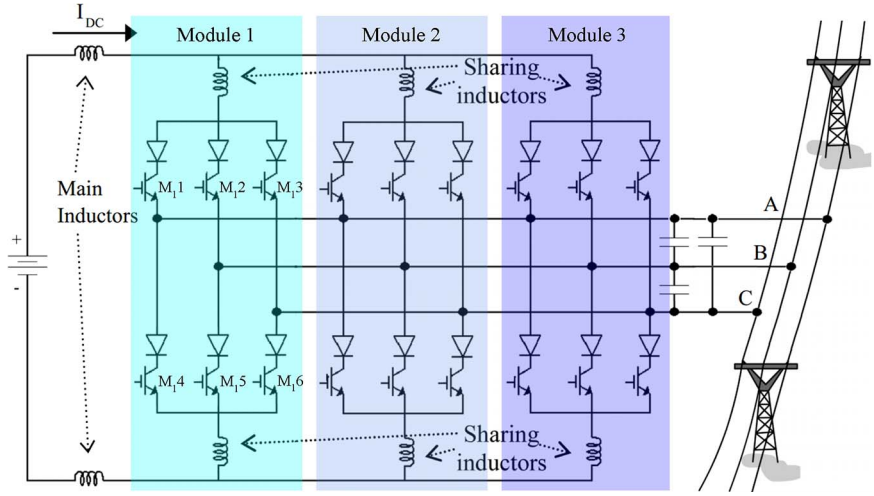

Fig. 2. Schematic of the MCSI.

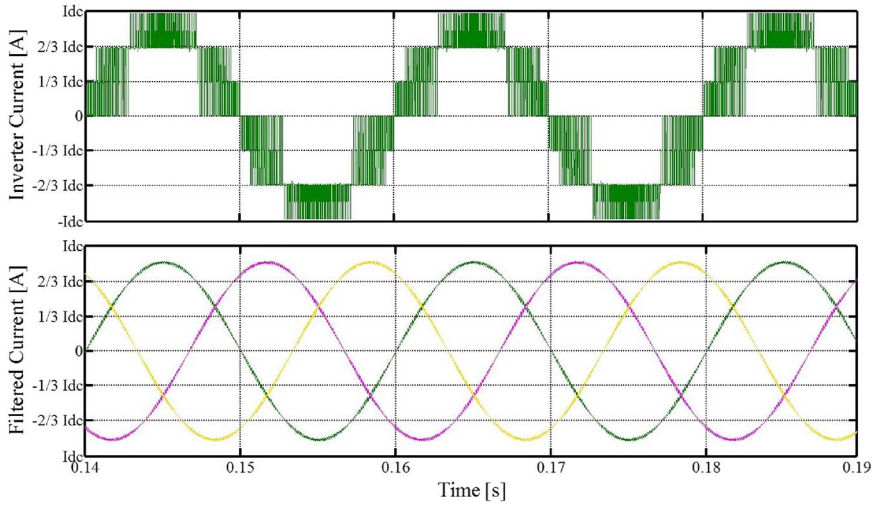

Fig. 3. Output current of the inverter. (Top) Phase-A unfiltered. (Bottom) Three phases filtered by the coupling capacitor bank.

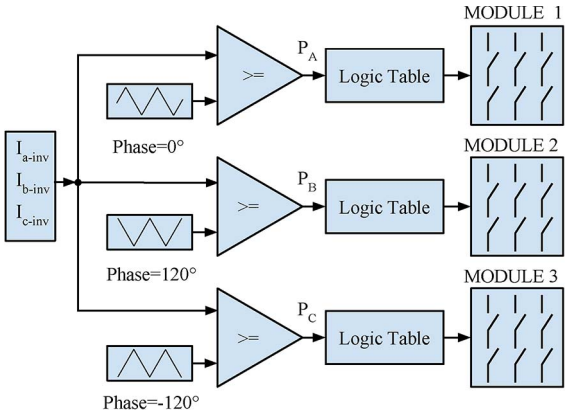

Fig. 4. Shifted carrier SPWM.

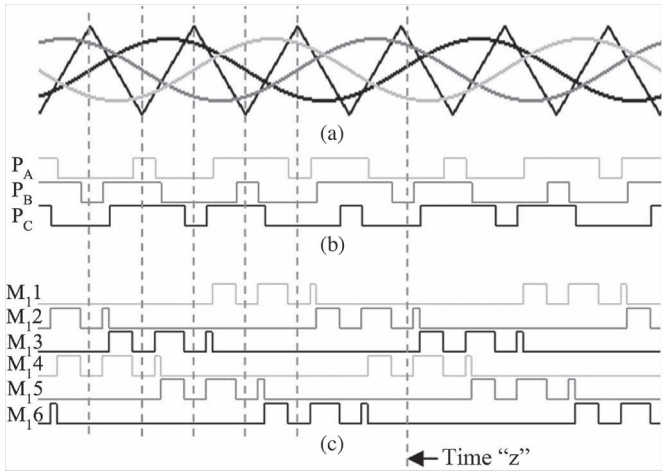

Fig. 5. Detail of the SPWM. Gate signals for one module.

currents dictates which of the six switches is currently having the biggest ON time. Hence, if the zero state which utilizes that switch is chosen, the number of switch commutations in a cycle can be minimized, reducing power dissipation and increasing efficiency. In this way, every possible zero state is used during a complete cycle; therefore, an active algorithm is used to perform this enhanced zero-state selection.

The minimum voltage required by the MCSI to be able to inject current to the grid is

$$V_{\text{source}} = \frac{3\sqrt{3}}{2\sqrt{2}} m_a V_{\text{phase}} \cos(\phi) \tag{1}$$

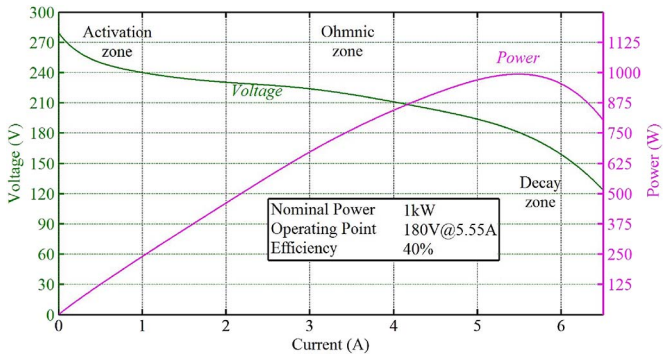

Fig. 6. Fuel cell current–voltage and power specifications.

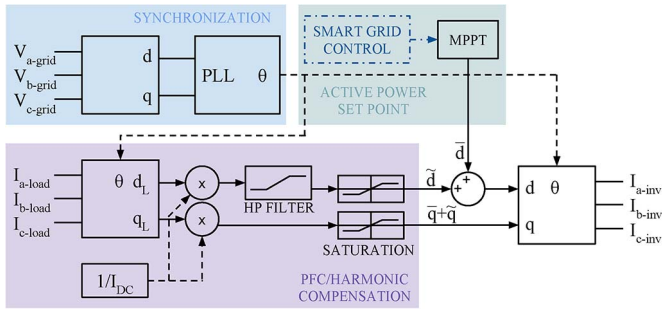

Fig. 7. Control scheme.

which is the result of equating input power with output power under an ideal no-loss condition. V_{phase} is the RMS phase voltage; m_a is the modulation index of the converter, ranging from 0 to 1; and ϕ is the phase difference between the main voltage and the injected current.

Although inductors are heavier and bulkier than capacitors, they have a higher mean time between failures (MTBF) and the failure mode is nonpolluting. Inductors can withstand high-voltage ripple without losing performance, and their characteristics hardly suffer from degradation, provided that they remain within their operating temperature range. This implies safer inverters with longer MTBF, less maintenance requirements, and a lower risk of pollution. In addition, inductors built with high-temperature superconductors will reduce losses appreciably, turning the MCSI into one of the most efficient solutions for multilevel inverters [24]. In addition, implementation of fault-tolerant topologies can be easily achieved by just adding a fourth module in a hot-spare configuration [22].

Moreover, multilevel topologies present several advantages regarding total harmonic distortion (THD) and stress on power switches and inductors or capacitors [25], [26]. Thus, multilevel converters are preferred against the standard solution with three-level topologies in spite of the increasing complexity of the circuit and control [24].

B. Fuel Cell

A fuel cell is an electrochemical device that converts chemical energy into electrical energy by means of a chemical reaction in an electrolyte, generating water and heat as waste [10]. In the proposed system, a PEM fuel cell is used because it is commercially available, providing many fuel cells manufactures and models ranging from low-end fuel cells to high-power systems.

The system is designed for a high-voltage cell with voltage versus current and power characteristics, as shown in Fig. 6, where three different operating areas can be noticed, namely, activation zone, ohmic zone, and decay zone. The best efficiency is achieved by operating in the ohmic region where the maximum power can be obtained [27]. The power versus voltage characteristic has a unique maximum point, which corresponds to the nominal power of the cell.

Several PEM models have been proposed [28], [29], but since this paper focuses primarily on system integration of fuel cells with the grid, a simple model with the V–I characteristics and first-order dynamics is good enough. This allows drastically reducing the time required by simulations without affecting the overall behavior and accuracy of the model. Due to the nonlinear relation between the voltage and current provided by the cell, a power converter must be used to set the desired operating point.

C. Control

The control block must fulfill five coordinated functions.

- Set the current drained from the cell to track the maximum power point of the cell stack (MPPT algorithm).
- Synchronize the MCSI with the grid.
- Generate the reference signals used for the modulation of the inverter I_{inv}.
- Adjust the active power delivered to the grid.
- Compensate reactive power and harmonics in the grid.

The MCSI modulation scheme, power factor and harmonic compensation, phase-locked loop (PLL), and the MPPT controller are implemented on a Xilinx FPGA. The design, simulation, and implementation are done using System Generator for DSP, a tool by Xilinx to deploy and simulate algorithms in the MATLAB/Simulink environment without the need to write any hardware description language code. This allows quickly developing and testing the modulation logic and control algorithms while saving development time.

The schematic of the developed control structure is shown in Fig. 7. To obtain the phase angle reference θ using a PLL algorithm, first, the grid voltage is transformed from *abc* to *dq0* reference frame using the Park transformation. The PLL is based on a fixed-point dual second-order generalized integrator PLL (DSOGI-PLL) as this implementation is one of the best solutions regarding setup time, steady-state error, and noise immunity [21]. The phase angle reference θ allows transforming the load currents from *abc* to *dq0* reference frame. The load current in *dq0* reference frame is then normalized to one by dividing the result of the Park transformation by the amount of dc current on the main inductor of the MCSI. This allows the modulation algorithm to work on a fixed scale, saving FPGA space and maximizing computing speed. The transformed components of the load current are d_L (active) and q_L (reactive). Hence, d_L correlates with active power, and q_L is proportional to the reactive power.

A high-pass filter removes the dc component of the d_L current, which is not necessary for the modulation of the MCSI. The mean value of the d reference current $\bar{d}$ is set by the MPPT or the smart grid control to supply active power to the grid. To avoid

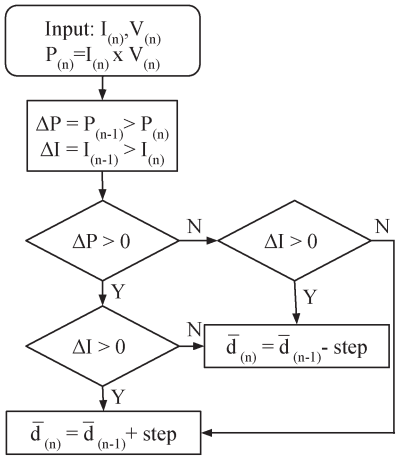

Fig. 8. MPPT algorithm.

saturation of the MCSI when entering in the overmodulation region, the current signals are limited to the maximum amount that can be provided by the MCSI without significantly increasing distortion in the output current. Finally, these signals are anti-transformed from *dq0* back to the *abc* reference frame where they are used as reference signals for the modulation of the MCSI.

The total active power the inverter supplies to the grid is composed of the active part of the harmonics present at the load plus the power provided by the fuel cell, which is controlled by the MPPT algorithm [30]. The reactive power measured at the load is directly fed to the MCSI controller, accomplishing power factor and harmonic compensation on the grid caused by the load.

The MPPT algorithm changes the active power reference of the system to track the maximum power point of the fuel cell in order to maximize the power delivered to the grid and increase the overall system performance. The MPPT is programmed in the FPGA with communication ports that allow a smart grid main control unit to adjust the amount of power delivered by the MCSI and the fuel cell in order to fit the operating conditions of the electric system, e.g., reducing or increasing active power momentarily in a distributed generation system when a change in wind speed is detected. This feature allows improving the dynamic response of the electric grid maximizing power quality and safety.

At startup, the main inductors of the inverter are discharged. To insure a soft start, the initial value of $\bar{d}$ is set to 1 in order to generate the least amount of zero states to reduce the speed of change on the current of the main inductors. As the inverter charges, the MPPT reduces the value of $\bar{d}$ to track the optimum power point of the fuel cell.

The MPPT algorithm flow diagram, as shown in Fig. 8, is based on a perturb and observe algorithm [31]. The derivatives of both power and current are calculated for each measurement, and based on the sign of these values, the $\bar{d}$ component is increased or decreased a fixed amount of 0.001 (0.1%) of the maximum current that the inverter can supply.

III. Simulation Results

Simulations were performed using the SimPowerSystem toolbox from MATLAB/Simulink, building a detailed model of all the components down to the transistor level, including

TABLE I
System Parameters

Parameter	Value
V_{grid}	$110V_{rms}$
Line frequency	50Hz
Main inductors	120mH
Sharing inductors	80mH
Capacitor Filter	470nF
IGBT Switching frequency	3150Hz
Output Switching frequency	9450Hz
Load	2kW+200VAr inductive
Fuel cell operating point	180V, 5.55A

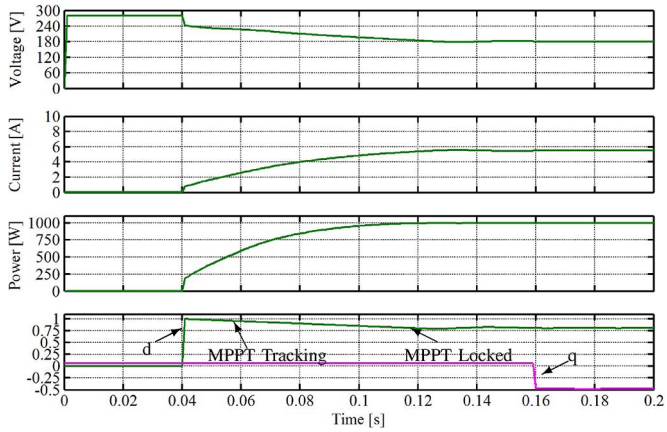

Fig. 9. Fuel cell voltage, current, power, and quadrature components of the current reference of the inverter.

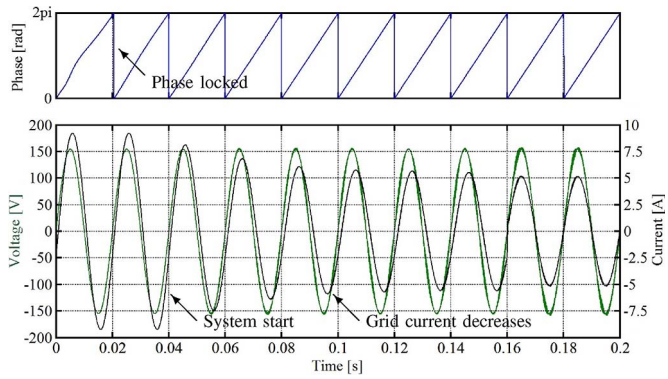

Fig. 10. Grid voltage and current of phase-A during startup.

dynamics and leakage components. Using this approach, the simulations lead to detailed and realistic results of the startup, steady state, the dynamic response of the system, and the activation of the power factor compensation (PFC) control. The simulation model represents the system presented in Fig. 1 with parameters detailed in Table I.

The simulation starts tracking the phase of the grid voltage in order to allow the PLL to stabilize, whereas the MCSI remains off by forcing the MPPT output to zero. Thus, the fuel cell provides no power to the grid. At 40 ms, the power reference of the MCSI is increased by turning on the MPPT algorithm, and at 160 ms, PFC is activated.

In Fig. 9, the fuel cell and reference signals of the MCSI are shown. The top two traces are the voltage and the current of the fuel cell stack, respectively. In the third trace, the power that the

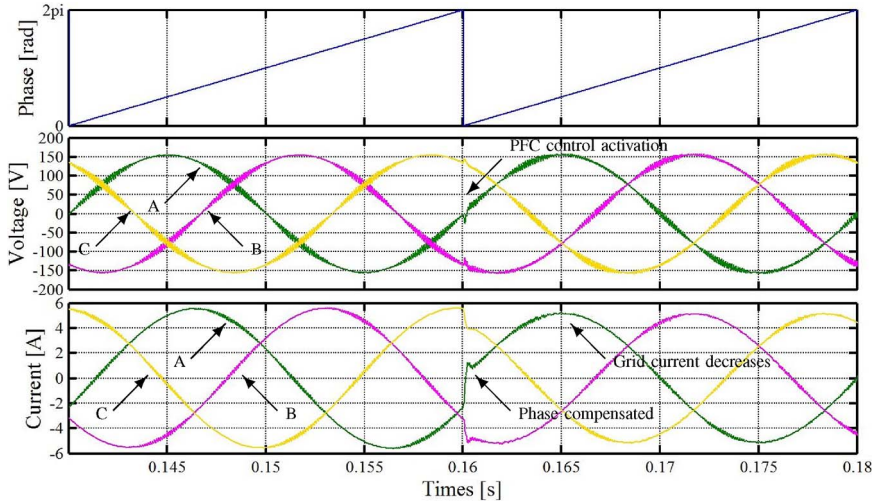

Fig. 11. Detail of PFC activation.

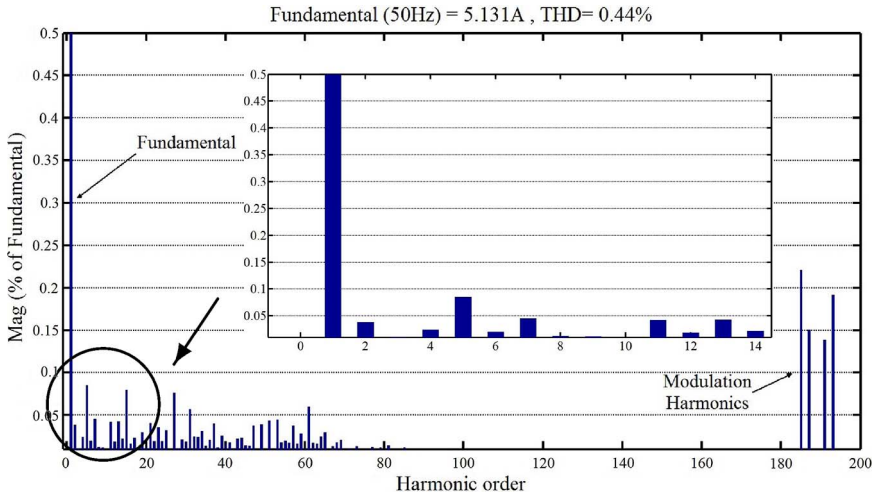

Fig. 12. Grid current THD.

fuel cell delivers is shown. The reference signals that control the inverter, i.e., d and q, are shown in the last plot. The MPPT controls the power reference until a steady state is achieved. The soft start forces a slow but steady increase in the output power, reaching maximum power tracking 80 ms after activation. As shown in Fig. 9, while the MPPT algorithm is active and locked, the output power of the cell has an insignificant ripple caused by the small change in voltage and current needed by the MPPT algorithm to calculate the power derivative. It is shown that the fuel cell provides up to 1 kW to the MCSI with a fast dynamic response.

The effects of the startup of the MCSI on grid voltages and currents are shown in Fig. 10. The upper trace shows the output of the PLL. A small transient disturbance can be seen in the first two periods until the PLL algorithm locks the line frequency and phase. The MCSI is started at 40 ms after grid phase is accurately tracked by the PLL. The fast response and high precision of the DSOGI-PLL avoids phase error propagation into the modulation, which could cause an increase in THD. In the bottom plot, the voltage and current of grid phase-A are shown. The distortion on grid voltage after the MCSI starts, at 0.04 s, is barely visible, below the acceptable limits established by IEEE Standard 519. The current decreases when the MCSI starts, reaching a steady value when the MPPT control is settled. At this time, the MCSI is delivering the power required by the smart grid, in this simulation case, full power of the fuel cell.

At time 0.16 s, the PFC control of the MCSI is activated. Fig. 11 shows the details of how the PFC is performed within milliseconds due to the high dynamics of the MCSI converter. The grid currents are settled and in phase with the grid in less than 2 ms. Grid currents are reduced as the power factor is compensated because the reactive power required by the load is being delivered by the MCSI.

Figs. 12 and 13 show the THD of grid current and voltage, respectively. Results are very promising since voltage THD at steady state is 0.71% and current THD is 0.44%. Both values are below 3% established by the IEC 61000-4-7 and the IEEE Standard 519. In both cases, the distortion is caused mainly by the switching harmonics. Since the MCSI consists of three identical modules to produce seven levels in the output current, the switching components are three times the commutation frequency of the transistors or $3m_f$ 50 Hz, where m_f is the frequency modulation index, in this case, taking a value of 63. The resulting switching frequency of the output current of the MCSI is 9450 Hz.

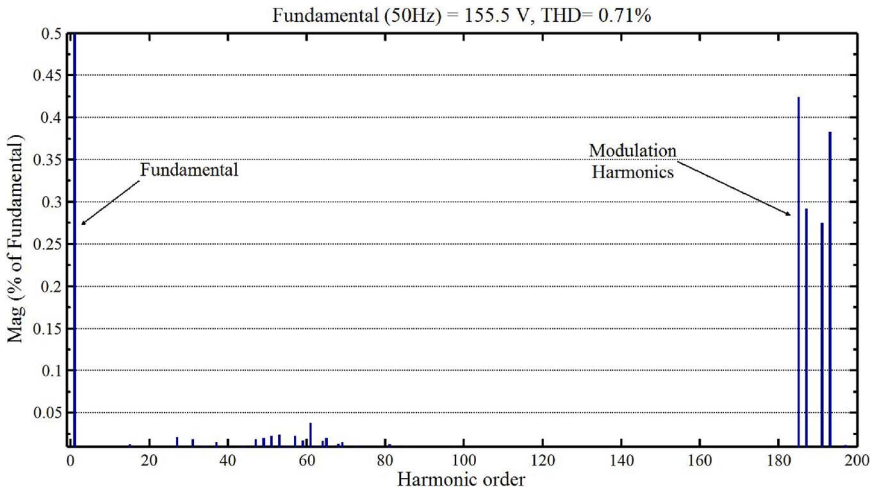

Fig. 13. Grid voltage THD.

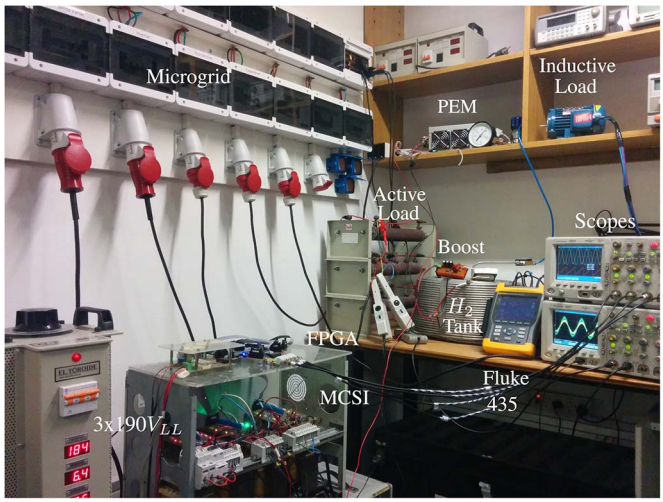

Fig. 14. Experimental setup.

IV. Experimental Results

To verify the behavior of the whole system, the experimental layout shown in Fig. 14 is built. A variable autotransformer is used at the laboratory as the microgrid source for the $3 \times 190\ V_{LL}$. The fuel cell used in this experiment, which is readily available at our facilities, is an H-200 PEM (FCS-C200) from Horizon Fuel Cell Technologies, is made of a stack of 40 cells, rated at 24 V and 8.3 A, giving a total of 199 W at its maximum operating point. The total load connected to the microgrid is composed of a wye-connected three-phase resistor of 121 Ω, accounting for 300 W of active power, and a reactive load of 150 var obtained using a commercial three-phase induction motor.

The nominal voltage of the cell used for the experimental results is several times lower than the dc voltage required by the MCSI. To emulate the behavior of the high-voltage fuel cell used in the simulations, a boost converter with a voltage gain of more than seven times must be used. A standard boost converter with an inductance of 400 μH, output capacitance of 47 μF, and switching frequency of 20 kHz is built. These values were chosen to provide an output voltage ripple smaller than 2% while keeping both conduction and switching losses low enough, improving efficiency. The duty cycle of the transistor is fixed at 86.7% to amplify the voltage from 24 to 180 V.

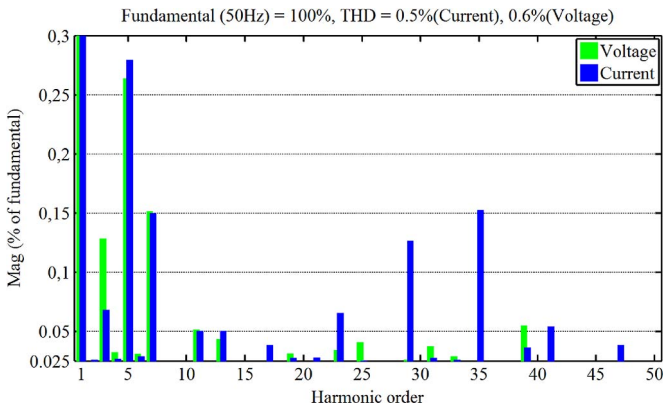

Fig. 15. Measured THD of grid voltage and current.

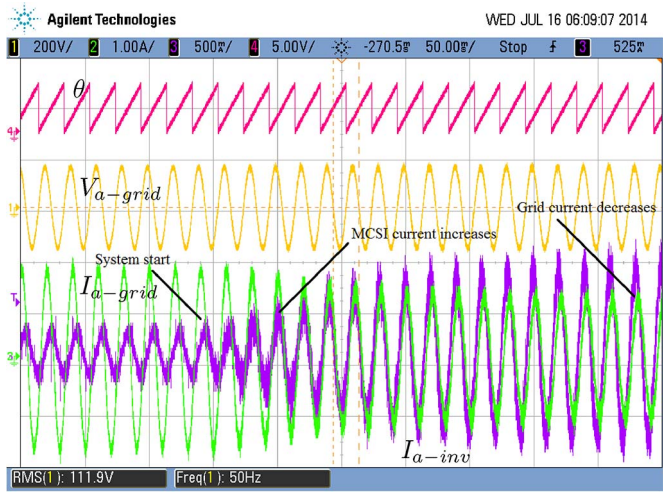

Fig. 16. System startup: (magenta) grid phase θ, (yellow) grid phase voltage $V_{a-\mathrm{grid}}$, (green) grid current $I_{a-\mathrm{grid}}$, and (violet) inverter current $I_{a-\mathrm{inv}}$.

To measure the THD of current i and voltage v, a Fluke 435 power quality analyzer is used. Both THD_v and THD_i values are below 0.6%, and their harmonic contents are shown in Fig. 15. The measurements of the startup are shown in Fig. 16 where

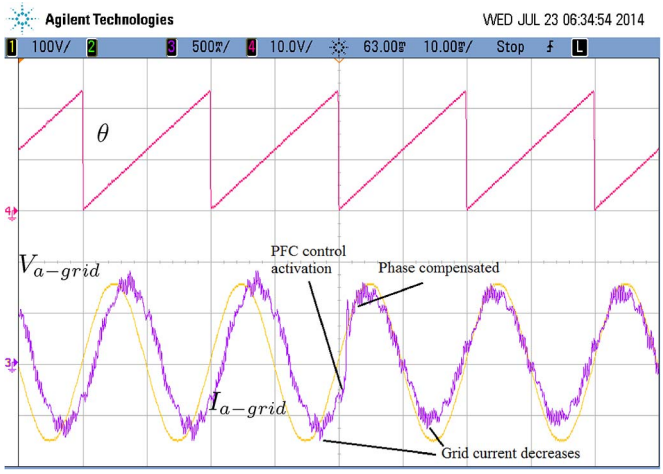

Fig. 17. PFC: (magenta) grid phase θ, (yellow) grid phase voltage $V_{a-\mathrm{grid}}$, and (violet) grid current $I_{a-\mathrm{grid}}$.

the grid phase is labeled θ. Phase-A grid voltage $V_{a-\mathrm{grid}}$ can be seen in the middle trace, whereas phase-A grid current $I_{a-\mathrm{grid}}$ and phase-A inverter current $I_{a-\mathrm{inv}}$ are superimposed on the bottom trace. The θ signal is calculated by the DSOGI-PLL algorithm using the measured grid phase voltages and showed on the oscilloscope by means of a digital-to-analog converter connected to the FPGA. This signal is shown to prove that the MCSI is properly following the phase of the grid voltage. The actual startup can be seen when $I_{a-\mathrm{inv}}$ increases while $I_{a-\mathrm{grid}}$ decreases simultaneously.

Fig. 17 shows the grid voltage and current when the PFC control is activated. The θ signal is in phase with the grid voltage $V_{a-\mathrm{grid}}$ even when grid current $I_{a-\mathrm{grid}}$ changes, showing excellent dynamic response of the PLL algorithm. Without compensation, $I_{a-\mathrm{grid}}$ lags $V_{a-\mathrm{grid}}$, whereas $I_{a-\mathrm{grid}}$ gets in phase with $V_{a-\mathrm{grid}}$ when compensation is activated. A decrease in $I_{a-\mathrm{grid}}$ can be appreciated as the reactive power is compensated. The fast performance of the PFC is shown in the experimental results in accordance with the simulations.

V. Conclusion

The integration of an MCSI and a fuel cell to provide energy and increase power quality in the electric grid has been presented. A system to deliver energy from a fuel cell to the electric grid using a seven-level MCSI power converter has been designed, evaluated through simulations, and implemented on a reduced scale model based on a 200-W fuel cell. The whole system shows an excellent behavior, both in simulation and experimental results. The MCSI output fulfills the IEEE Standard 519 and the IEC 61000-4-7 standard regarding harmonics distortion. All the experimental results demonstrate that the experimental setup has a good correlation compared with the simulation counterpart, allowing to extrapolate the results obtained to much higher power systems. The proposed system is a good choice in distributed generation systems or smart grids as it can provide active power while compensating power factor and harmonic distortion on the grid current. The proposed energy integration system is also suitable to integrate different energy sources such as wind or solar using the same layout, requiring only minimal changes in the control block.

References

[1] S. Motapon, L.-A. Dessaint, and K. Al-Haddad, "A comparative study of energy management schemes for a fuel-cell hybrid emergency power system of more-electric aircraft," *IEEE Trans. Ind. Electron.*, vol. 61, no. 3, pp. 1320–1334, Mar. 2014.

[2] T. Zhou and B. Francois, "Energy management and power control of a hybrid active wind generator for distributed power generation and grid integration," *IEEE Trans. Ind. Electron.*, vol. 58, no. 1, pp. 95–104, Jan. 2011.

[3] B. Belvedere *et al.*, "A microcontroller-based power management system for standalone microgrids with hybrid power supply," *IEEE Trans. Sustain. Energy*, vol. 3, no. 3, pp. 422–431, Jul. 2012.

[4] L. Garcia *et al.*, "Dual transformerless single-stage current source inverter with energy management control strategy," *IEEE Trans. Power Electron.*, vol. 28, no. 10, pp. 4644–4656, Oct. 2013.

[5] C. Kunusch, P. Puleston, M. Mayosky, and A. Husar, "Control-oriented modeling and experimental validation of a PEMFC generation system," *IEEE Trans. Energy Convers.*, vol. 26, no. 3, pp. 851–861, Sep. 2011.

[6] Y.-C. Chang, C.-L. Kuo, K.-H. Sun, and T.-C. Li, "Development and operational control of two-string maximum power point trackers in dc distribution systems," *IEEE Trans. Power Electron.*, vol. 28, no. 4, pp. 1852–1861, Apr. 2013.

[7] E. Ribeiro, A. Marques Cardoso, and C. Boccaletti, "Fuel cell supercapacitor system for telecommunications," in *Proc. IET Int. Conf. Power Electron., Mach. Drives*, Apr. 2010, pp. 1–6.

[8] S. Anand, S. Gundlapalli, and B. Fernandes, "Transformer-less grid feeding current source inverter for solar photovoltaic system," *IEEE Trans. Ind. Electron.*, vol. 61, no. 10, pp. 5334–5344, Oct. 2014.

[9] T. Kawaguchi, T. Sakazaki, T. Isobe, and R. Shimada, "Offshore-wind-farm configuration using diode rectifier with MERS in current link topology," *IEEE Trans. Ind. Electron.*, vol. 60, no. 7, pp. 2930–2937, Jul. 2013.

[10] M. Aguirre and M. Valla, "An environmental friendly alternative for hydrogen production and electric energy generation," in *Proc. IEEE Conf. Ind. Electron.*, Nov. 2011, pp. 3099–3104.

[11] S.-J. Cheng, Y.-K. Lo, H.-J. Chiu, and S.-W. Kuo, "High-efficiency digital-controlled interleaved power converter for high-power PEM fuel cell applications," *IEEE Trans. Ind. Electron.*, vol. 60, no. 2, pp. 773–780, Feb. 2013.

[12] B. Somaiah and V. Agarwal, "Recursive estimation-based maximum power extraction technique for a fuel cell power source used in vehicular applications," *IEEE. Trans. Power Electron.*, vol. 28, no. 10, pp. 4636–4643, Oct. 2013.

[13] R. Praveen and K. Latha, "Comparison of various MPPT techniques for different fuel flow," in *Proc. Int. Conf. Energy Efficient Technol. Sustain.*, Apr. 2013, pp. 540–545.

[14] D. Kanchan and N. Hadagali, "Bidirectional dc/dc converter system for solar and fuel cell powered hybrid electric vehicle," in *Proc. Int. Conf. Emerging Res. Areas: Magn., Mach. Drives*, Jul. 2014, pp. 1–6.

[15] M. Aguirre, L. Calvino, and M. Valla, "Multilevel current-source inverter with FPGA control," *IEEE Trans. Ind. Electron.*, vol. 60, no. 1, pp. 3–10, Jan. 2013.

[16] G. Grandi, J. Loncarski, and O. Dordevic, "Analysis and comparison of peak-to-peak current ripple in two-level and multilevel PWM inverters," *IEEE Trans. Ind. Electron.*, vol. 62, no. 5, pp. 2721–2730, May 2015.

[17] L. Franquelo *et al.*, "The age of multilevel converters arrives," *IEEE Ind. Electron. Mag.*, vol. 2, no. 2, pp. 28–39, Jun. 2008.

[18] K. Hatua and V. T. Ranganathan, "A novel VSI- and CSI-fed dual stator induction motor drive topology for medium-voltage drive applications," *IEEE Trans. Ind. Electron.*, vol. 58, no. 8, pp. 3373–3382, Aug. 2011.

[19] L. Hadjidemetriou, E. Kyriakides, and F. Blaabjerg, "A robust synchronization to enhance the power quality of renewable energy systems," *IEEE Trans. Ind. Electron.*, to be published.

[20] V. Sáez *et al.*, "FPGA implementation of grid synchronization algorithms based on DSC, DSOGI QSG and PLL for distributed power generation systems," in *Proc. IEEE Int. Symp. Ind. Electron.*, 2010, pp. 2765–2770.

[21] P. Cossutta, M. Aguirre, M. Engelhardt, A. Cao, and M. Valla, "High speed fixed point DSOGI PLL implementation on FPGA for synchronization of grid connected power converters," in *Proc. IEEE Int. Symp. Ind. Electron.*, Jun. 2014, pp. 1372–1377.

[22] M. Aguirre, L. Calviño, and M. Valla, "Fault tolerant multilevel current source inverter," in *Proc. IEEE Int. Conf. Ind. Tech.*, Mar. 2010, pp. 1345–1350.

[23] Z. Bai and Z. Zhang, "Conformation of multilevel current source converter topologies using the duality principle," *IEEE Trans. Power Electron.*, vol. 23, no. 5, pp. 2260–2267, Sep. 2008.
[24] N. Murray, J. Arrillaga, N. Watson, and Y. Liu, "Four quadrant multilevel current source power conditioning for superconductive magnetic energy storage," in *Proc. Australasian Univ. Power Eng. Conf.*, 2009, pp. 1–5.
[25] J. Barros and J. Silva, "Optimal predictive control of three-phase NPC multilevel converter for power quality applications," *IEEE Trans. Ind. Electron.*, vol. 55, no. 10, pp. 3670–3681, Oct. 2008.
[26] J. Rodriguez *et al.*, "Multilevel converters: An enabling technology for high-power applications," *Proc. IEEE*, vol. 97, no. 11, pp. 1786–1817, Nov. 2009.
[27] S. Sirisukprasert and T. Saengsuwan, "The modeling and control of fuel cell emulators," in *Proc. Int. Conf. Electr. Eng./Electron., Comput., Telecommun. Inf. Technol.*, vol. 2, May 2008, pp. 985–988.
[28] W. Friede, S. Rael, and B. Davat, "Mathematical model and characterization of the transient behavior of a PEM fuel cell," *IEEE Trans. Power Electron.*, vol. 19, no. 5, pp. 1234–1241, Sep. 2004.
[29] M. Ellis, M. Von Spakovsky, and D. Nelson, "Fuel cell systems: Efficient, flexible energy conversion for the 21st century," *Proc. IEEE*, vol. 89, no. 12, pp. 1808–1818, Dec. 2001.
[30] M. Aguirre, L. Calviño, V. Corasaniti, and M. Valla, "Multilevel current source inverter to improve power quality in a distribution network," in *Proc. IEEE Int. Symp. Ind. Electron.*, Jul. 2010, pp. 3292–3297.
[31] M. Taghikhani and I. Soltani, "A new maximum power point tracking control method of proton exchange membrane fuel cell's system," in *Proc. Electr. Power Distrib. Netw.*, May 2012, pp. 1–7.

Pablo Cossutta (M'12) received the Electronics Engineer degree (with honors) and the Specialist on Medical Equipment degree from the Instituto Tecnológico de Buenos Aires (ITBA), Buenos Aires, Argentina, in 2001 and 2004, respectively, where he is currently working toward the Ph.D. degree in power electronics.

He is also an Associate Professor with ITBA, where he is engaged in teaching and research on power and industrial electronics.

Miguel Pablo Aguirre (M'09) received the Electronics Engineer degree from the Instituto Tecnológico de Buenos Aires (ITBA), Buenos Aires, Argentina, in 1995 and the Ph.D. degree from the Universidad Nacional de La Plata, La Plata, Argentina, in 2013.

He is currently a Full Professor with and the Head of the Department of Electrical and Electronics Engineering, ITBA, where he is also engaged in teaching and research on power electronics, power quality, and renewable energy sources.

Andrés Cao received the Electronics Engineer degree (with honors) from the Instituto Tecnológico de Buenos Aires (ITBA), Buenos Aires, Argentina, in 2014.

He is currently a Project Engineer with the Research and Development Center on Industrial Electronics (CIDEI), ITBA, where he conducts research on power and industrial electronics and interfaces. He is also an Assistant Professor with ITBA.

Santiago Raffo (M'14) received the Electronics Engineer degree from the Instituto Tecnológico de Buenos Aires (ITBA), Buenos Aires, Argentina, in 2014.

He is currently a Project Engineer with the Research and Development Center on Industrial Electronics (CIDEI), ITBA, where he conducts research on power current-source inverters for industrial applications.

María Inés Valla (S'79–M'80–SM'97–F'10) received the Electronics Engineer and Doctor in Engineering degrees from the National University of La Plata (UNLP), La Plata, Argentina, in 1980 and 1994, respectively.

She is currently a Full Professor with the Department of Electrical Engineering, Faculty of Engineering, UNLP. She is also with the Consejo Nacional de Investigaciones Científicas y Técnicas (CONICET), Buenos Aires, Argentina. She is engaged in teaching and research on power converters, power quality, and renewable energy sources.

Prof. Valla is a member of the Buenos Aires Academy of Engineering in Argentina, the IEEE Fellows Committee, and the IEEE Power System Medal Committee. She is a Co-Editor-in-Chief of the IEEE TRANSACTIONS ON INDUSTRIAL ELECTRONICS.